Isotopic diffusion in polycrystalline ice

ALAN W. REMPEL,[1] J. S. WETTLAUFER [2]

[1]*Division of Engineering and Applied Sciences, Harvard University, Cambridge, Massachusetts 02138, U.S.A.*
E-mail: rempel@esag.harvard.edu
[2]*Department of Physics, Yale University, New Haven, Connecticut 06520-8120, U.S.A.*

ABSTRACT. Quantitative ice-core paleoclimatology must account for post-depositional processes, such as vapor-phase diffusion in the firn. After pore close-off, diffusion continues to smooth the stable-isotope records $\delta^{18}O$ and δD that are eventually recovered from the ice, leading to the loss of high-frequency information. Johnsen and others (1997) found much higher rates of diffusive smoothing in the Greenland Icecore Project (GRIP) Holocene ice than would be predicted by diffusion through solid ice alone, and Nye (1998) argued that transport through liquid veins might explain this apparent *excess* diffusion. However, the analysis of Johnsen and others (2000) indicates that the required vein dimensions may be unrealistically large. Here, we model the diffusion of stable isotopes in polycrystalline ice and show that the predictions of Nye (1998) and those of Johnsen and others (2000) actually represent two end-members in a range of potential behavior. Our model determines which of these asymptotic regimes more closely resembles the prevailing conditions and quantifies the role of pre-melted liquid in the smoothing of isotopic signals. The procedure thereby ties together the two approaches and provides a rostrum for accurate analysis of isotope records and paleotemperature reconstructions.

LIST OF SYMBOLS

Second column indicates units (K: temperature; L: length; M: mass; T: time).

a	L	Vein radius
b	L	Grain radius
d	L	Film thickness
D	$L^2 T^{-1}$	Molecular diffusivity
f		Enhancement factor
F		Radial shape factor (see Equation (15))
F_v		Liquid concentration scaling factor
g	LT^{-2}	Acceleration of gravity
h	LT^{-1}	Accumulation rate
H	L	Ice-sheet thickness
k	L^{-1}	Wavenumber
M		Total number of harmonic components
N	L^{-3}	Number density of major species
N'	L^{-3}	Number density of minor species
Pe		Péclet number (see Equation (A1))
r	L	Radial coordinate
S	L^{-3}	Standard isotopic ratio
$\mathbf{S}$	L^2	Surface of integrating volume
t	T	Time
T	K	Temperature
U	LT^{-1}	Darcy transport velocity
v	LT^{-1}	Average velocity of water
z	L	Axial coordinate
α		Fractionation constant
δ		Delta value (see Equation (8))
Δ	L	Integrating-volume height
$\dot{\epsilon}$	T^{-1}	Vertical strain rate
η	T	Dummy variable
λ	L	Wavelength

ν	$ML^{-1}T^{-1}$	Viscosity
Π	L^2	Permeability
ρ	ML^{-3}	Density
σ	L	Diffusion length
τ	T	Dummy variable
τ_1		Tortuosity factor
Υ		Dimensionless parameter (see Equation (21))
ϕ		Liquid volume fraction
χ		Permeability factor
Ω	L^3	Integrating volume

Subscripts:

0	Initial value
i	Harmonic-component index
J	Johnsen-model prediction
N	Nye-model prediction
r	Radial
s	Solid
v	Liquid (vein)
z	Axial

1. INTRODUCTION

The stable-isotope ratios $\delta^{18}O$ and δD measured in ice from polar cores provide detailed records of past temperature (Dansgaard, 1964; Johnsen and others, 1997; Petit and others, 1999). The isotope records themselves are smoothed by diffusion at a rate that is enhanced by connected vapor pathways in the firn (Johnsen, 1977; Whillans and Grootes, 1985). Several inversion methods have been developed to account for this post-depositional alteration and recover the original isotopic signals (Johnsen, 1977; Cuffey and Steig, 1998; Bolzan and Pohjola, 2000). Seasonal variations are of particular

interest, both for their importance to our understanding of climate dynamics and for their use in absolute dating. Beneath the level of pore close-off, post-depositional alteration is slowed considerably. Nevertheless, diffusion continues to smooth the isotope records, leading to the loss of seasonal and other high-frequency information. In fact, Johnsen and others (1997) found that, in the deep Greenland ice sampled by the Greenland Icecore Project (GRIP) core, the rate of smoothing is considerably faster than would be predicted by diffusion through solid ice alone. Intriguingly, this apparent *excess* diffusion appears to apply only within the Holocene ice at GRIP; the rate of alteration within ice from the Wisconsin glacial period is consistent with the normal solid-state diffusivity. Nye (1998) argued that the presence of liquid veins at the boundaries of ice grains (Nye and Frank, 1973; Mader, 1992a, b; Nye, 1992) might explain the excess diffusion. However, the analysis of Johnsen and others (2000) suggests that the required vein dimensions are unrealistically large. Here, we model the diffusion of stable isotopes in polycrystalline ice and show that the predictions of Nye (1998) and those of Johnsen and others (2000) represent two end-members of a more general range of behavior. We identify the physical characteristics that determine which of these asymptotic regimes more closely resembles the prevailing conditions and quantify the role of liquid in the smoothing of isotopic signals. A deeper understanding of the processes by which the isotope records evolve will help to increase the accuracy and resolution of paleotemperature reconstructions.

In polycrystalline ice that is below the normal bulk-melting temperature of 0°C, veins of *pre-melted* liquid trace the triple junctions between three grains and join at nodes where four ice grains meet (Nye and Frank, 1973). The veins and nodes constitute a connected liquid network that is prevented from freezing at sub-zero temperatures by two physical effects. First, the surface energy of the solid–liquid interface favors the presence of liquid as the curvature of the vein walls increases; this is the Gibbs–Thomson effect. Second, soluble impurities that are rejected from the ice lattice are concentrated in the liquid and reduce its chemical potential so that it remains in equilibrium with the solid at colder temperatures. Intermolecular interactions between adjacent ice grains or between the ice and a foreign substance such as a gas bubble or a dust particle are a third cause of pre-melting that can also contribute to the total quantity of liquid present (Ohtomo and Wakahama, 1983; Dash and others, 1995; Wettlaufer, 1999; Wettlaufer and Dash, 2000). The liquid network facilitates the transport of soluble impurities and assists the purification of temperate ice (Glen and others, 1977; Mader, 1992b). In polar ice, the diffusion of soluble impurities through the liquid network can influence the compositional records recovered from ice cores (Rempel and others, 2001, 2002; Rempel and Wettlaufer, 2003) and enhance the potential for chemical reactions to take place (Fisher, 1987). Here we examine how pre-melted liquid affects the stable-isotope records beneath the firn.

Nye (1998) proposed his model, referred to here as the *Nye* model, immediately after Johnsen discussed his observations at a NATO Advanced Study Institute in 1997 (Johnsen and others, 1999). In the Nye model, diffusion through the vein liquid is treated as instantaneous and the rate of diffusive smoothing is determined by the exchange of isotopes between the solid grains and the liquid veins. Adopting parameter values that represent conditions typical of the GRIP Holocene ice, the model predictions reproduce the
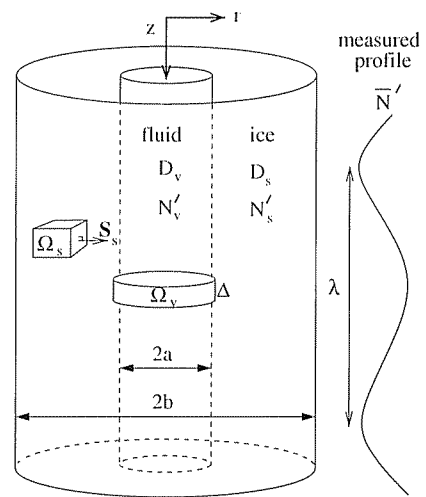

Fig. 1. The geometry used to model the vein-mediated diffusion of stable isotopes through polycrystalline ice (see text for details).

order-of-magnitude increase in apparent diffusivity that Johnsen and others (1997) inferred from the data. Existing inversion algorithms, which might be used to recover the original isotope record, cannot be applied directly to the Nye model. Johnsen and others (2000) addressed this issue by developing an alternative formulation for vein-mediated isotopic diffusion, referred to here as the *Johnsen* model, which produces predictions that are at odds with the Nye-model results. In particular, using parameter values that correspond to those adopted by Nye, the Johnsen model predicts a more modest three-fold increase to the apparent diffusivity. The Johnsen model is based on earlier treatments of isotopic diffusion in the firn (Johnsen, 1977; Whillans and Grootes, 1985), with the liquid network playing the role that the vapor phase takes higher up in supplying fluid pathways for rapid diffusion. The ice grains and the vein liquid at each depth are assumed to be in local isotopic equilibrium and the rate of diffusive smoothing is controlled by diffusion through the fluid phase. It is worth noting here that the rate of signal alteration in the Nye model is independent of the liquid diffusivity, while the Johnsen-model predictions are insensitive to the diffusivity of the solid. The model we present here simulates the entire process including both the exchange of isotopes between the phases and the rapid transport through the fluid. We begin by presenting a basic model that illuminates the essential physics using the geometry considered by Nye (1998). We then generalize the model to simulate the conditions sampled by ice cores, and examine the evolution of an arbitrary initial signal that is subject to the effects of vertical strain. Informed by comparisons between the model predictions and ice-core observations, we discuss possible causes of the apparent excess diffusion and suggest directions for further research.

2. THE MODEL

To provide physical insight, we seek an analytical description of isotopic diffusion in the model system shown in Figure 1. A cylindrical annulus of ice with outer radius b, chosen to correspond to the grain radius (typically $b = O$ (10^{-3}) m), envelops a fluid cylinder of radius a that represents a vein (typically $a = O$ (10^{-6}) m). The radially averaged volumetric concentration $\bar{N}'$ of the minor isotope (^{18}O or D) displays an

initial periodic signal with wavelength λ in the axial direction. This averaged signal can be thought of as representing the measured seasonal variations in the isotope content of ice-core samples. To predict the evolution of the isotope profile, we proceed by examining the conservation conditions in each phase.

In the solid outer cylinder, we consider an arbitrary control volume Ω_s with surface S_s, shown schematically in Figure 1. Diffusion across the surface of the control volume changes the number of molecules of the minor species contained within it, so the evolution of the number density of the minor isotopic species N' is described by

$$\frac{\partial}{\partial t} \int_{\Omega_s} N'_s \, d\Omega_s = \int_{S_s} D_s \nabla N'_s \cdot d\mathbf{S_s} \, , \qquad (1)$$

where D is the molecular diffusivity and the subscript s refers to the solid. The divergence theorem is applied to the right side and we note that the integration volume is arbitrary so that

$$\frac{\partial N'_s}{\partial t} = D_s \nabla^2 N'_s = D_s \left(\frac{\partial^2 N'_s}{\partial r^2} + \frac{1}{r} \frac{\partial N'_s}{\partial r} + \frac{\partial^2 N'_s}{\partial z^2} \right) \, , \qquad (2)$$

where the radial r and axial z coordinates are indicated in Figure 1. A no-flux condition holds along the outer boundary so that

$$\left. \frac{\partial N'_s}{\partial r} \right|_{r=b} = 0 \, . \qquad (3)$$

The condition along the inner boundary where $r = a$ is found by matching with the isotope concentration in the fluid phase, to be examined next.

The vein is sufficiently narrow that the concentration in the fluid depends only on z. Accordingly, we consider the conditions for isotope conservation in a disk-shaped control volume Ω_v of height Δ and radius $a + \Delta$ that spans the vein cross-section, as shown in Figure 1. We confine our discussion to a purely diffusive parameter regime; scaling arguments that elucidate the conditions under which fluid flow through the vein system is an important transport mechanism are provided in the Appendix. Changes in the isotope content are accomplished by diffusion down the axial fluid-concentration gradient and exchange with the solid ice across the phase boundary at $r = a$ so that

$$\frac{\partial}{\partial t} \int_{\Omega_v} N'_v \, d\Omega_v = \int_{S_v} D_v \nabla N'_v \cdot d\mathbf{S_v} + \int_{S_v} D_s \nabla N'_s \cdot d\mathbf{S_v} \, , \qquad (4)$$

where the subscript v refers to the vein liquid. The final term in Equation (4) accounts for the diffusive exchange between the ice and the vein fluid that is driven by gradients in the isotopic content of the solid $\nabla N'_s$ at the radial boundary of Ω_v. The divergence theorem is applied to the first surface integral and each term is integrated as Δ tends to zero so that, to leading order in Δ, Equation (4) becomes

$$\pi a^2 \Delta \frac{\partial N'_v}{\partial t} = \pi a^2 \Delta D_v \frac{\partial^2 N'_v}{\partial z^2} + 2\pi a \Delta D_s \left. \frac{\partial N'_s}{\partial r} \right|_{r=a} \, . \qquad (5)$$

Isotopic equilibrium between the fluid and the solid along their common boundary implies that

$$N'_v = \left. \frac{N_v}{\alpha N_s} N'_s \right|_{r=a} \, , \qquad (6)$$

where N represents the concentration of the major species (^{16}O or H) and the fractionation coefficient α is close to

unity. We substitute Equation (6) into Equation (5) and use Equation (2) to eliminate the time derivative so that

$$\left. \frac{\partial^2 N'_s}{\partial r^2} \right|_{r=a} + \frac{N_v - 2\alpha N_s}{N_v a} \left. \frac{\partial N'_s}{\partial r} \right|_{r=a} + \left(1 - \frac{D_v}{D_s} \right) \left. \frac{\partial^2 N'_s}{\partial z^2} \right|_{r=a} = 0 \, . \qquad (7)$$

This is the second boundary condition that solutions to Equation (2) must satisfy.

In ice-core studies the isotope concentrations are normally reported as δ values, which are defined in terms of the standard ratio S according to

$$N'_s = N_s S(1 + \delta) \, . \qquad (8)$$

Noting that $D_v \gg D_s$, $\alpha \approx 1$ and the ratio N_s/N_v is approximately equal to the ratio of the solid and liquid densities $\rho_s/\rho_v \approx 1$, we transform variables and write the governing Equation (2) and its boundary conditions (3) and (7) as

$$\frac{\partial \delta}{\partial t} = D_s \left(\frac{\partial^2 \delta}{\partial r^2} + \frac{1}{r} \frac{\partial \delta}{\partial r} + \frac{\partial^2 \delta}{\partial z^2} \right) \, , \qquad (9)$$

$$\left. \frac{\partial \delta}{\partial r} \right|_{r=b} = 0 \, , \qquad (10)$$

and

$$\left. \frac{\partial^2 \delta}{\partial r^2} \right|_{r=a} - \frac{1}{a} \left. \frac{\partial \delta}{\partial r} \right|_{r=a} - \frac{D_v}{D_s} \left. \frac{\partial^2 \delta}{\partial z^2} \right|_{r=a} = 0 \, . \qquad (11)$$

The volume fraction of liquid is much less than unity so that $b \gg a$ and the radially averaged initial condition can be written as

$$\left. \bar{\delta} \right|_{t=0} \approx \frac{2}{b^2} \int_a^b r \delta \, dr = \delta_0 + \delta_1 \cos(k_z z) \, , \qquad (12)$$

where $k_z = 2\pi/\lambda$ is the wavenumber of the axial isotopic variations, and δ_0 and δ_1 are the mean value and amplitude of the initial signal. Equations (9–12) constitute a complete description of isotopic diffusion in the model system.

We use separation of variables and write the solution to Equation (9) that satisfies Equations (10–12) as

$$\delta = \delta_0 + \delta_1 F(r) \cos(k_z z) \exp \left[-\left(1 + \frac{k_r^2}{k_z^2} \right) k_z^2 D_s t \right] \, , \qquad (13)$$

where the radial wavenumber k_r is found as the solution to the following transcendental equation:

$$J_1(k_r a) Y_1(k_r b) - J_1(k_r b) Y_1(k_r a) \qquad (14)$$
$$= \left(\frac{a k_r}{2} - \frac{a k_z^2 D_v}{2 k_r D_s} \right) [J_0(k_r a) Y_1(k_r b) - J_1(k_r b) Y_0(k_r a)] \, .$$

The radial dependence of the isotopic composition is expressed in terms of the Bessel functions J and Y as

$$F(r) = \frac{b^2 k_r}{2a} \frac{J_0(k_r r) Y_1(k_r b) - J_1(k_r b) Y_0(k_r r)}{J_1(k_r b) Y_1(k_r a) - J_1(k_r a) Y_1(k_r b)} \, , \qquad (15)$$

which averages to $\bar{F} = 2/b^2 \int_a^b r F \, dr = 1$. Equation (13) predicts that the presence of veins in polycrystalline ice causes a harmonic signal with wavenumber k_z to be attenuated at a rate equivalent to that in a homogeneous medium with an effective diffusivity that is $f = 1 + k_r^2/k_z^2$ times greater than the molecular diffusivity in an ice monocrystal D_s. The *enhancement factor* f provides a convenient measure of the effect of pre-melted liquid on the diffusion of stable isotopes. Equation (13) can also be written in terms of a diffusion
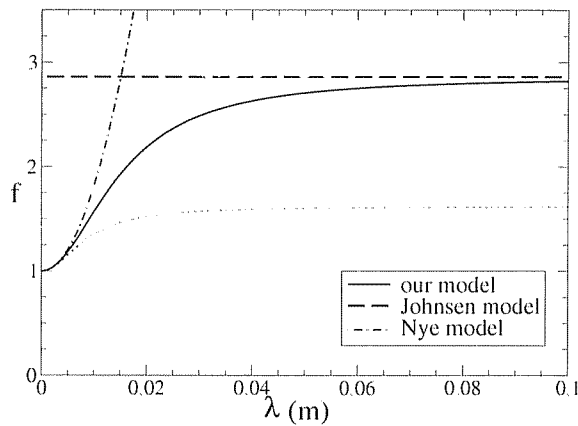
Fig. 2. The enhancement factor f as a function of wavelength $\lambda = 2\pi/k_z$ for the present model (solid line), the Nye model (dot-dashed line) and the Johnsen model (dashed line). The dotted line shows the predicted enhancement when the liquid diffusivity is reduced by a factor of $\tau_1 = 3$. The temperature $T = 241$ K, the vein radius $a = 10^{-6}$ m and the grain-size $b = 10^{-3}$ m.

length $\sigma = \sqrt{2fD_s t}$ that describes the smoothing effects so that

$$\delta = \delta_0 + \delta_1 F(r) \cos(k_z z) \exp\left(-\frac{1}{2} k_z^2 \sigma^2\right). \quad (16)$$

Signals with wavelengths that are comparable to or smaller than the diffusion length are smoothed significantly, whereas those with much longer wavelengths retain their initial form.

2.1. Model predictions

2.1.1. The Nye model

It is useful to compare our predictions with those of the Nye and Johnsen models. The Nye model proceeds from the observation that $D_v \gg D_s$ and examines the limiting case in which the fluid diffusivity may be treated as infinite so that the flux boundary condition given in Equation (11) is replaced by $\delta|_{r=a} = \delta_0$. The predicted evolution of δ can be expressed in the same manner as the model presented here, except with the radial wavenumber k_r in Equations (13) and (15) replaced by k_N, which satisfies

$$J_0(k_N a)Y_1(k_N b) - J_1(k_N b)Y_0(k_N a) = 0, \quad (17)$$

which is the natural consequence of $D_v \gg D_s$ in Equation (14). Significantly, Equation (17) indicates that k_N is insensitive to the temperature-dependent diffusivities D_v and D_s, and the axial wavenumber k_z. The Nye model can also be written in the form of Equation (16), with the diffusion length modified so that $\sigma_N = \sqrt{2f_N D_s t}$, where the corresponding enhancement factor is defined as $f_N = 1 + k_N^2/k_z^2$.

2.1.2. The Johnsen model

The Johnsen model treats the case in which radial variations in isotope concentration are negligible and all transport takes place through the fluid. For the purposes of comparison with our model results, this second assumption is relaxed to allow axial concentration gradients to drive diffusion through the solid as well as the fluid. The appropriate governing equation is readily obtained from considerations similar to those that

led to Equation (4), but with the integrating volumes encompassing a thin slice through both cylinders so that

$$\pi b^2 \frac{\partial \delta}{\partial t} \approx \pi a^2 D_v \frac{\partial^2 \delta}{\partial z^2} + \pi b^2 D_s \frac{\partial^2 \delta}{\partial z^2}. \quad (18)$$

The assumption of equilibrium between the phases in the Johnsen model implies that $F_J(r) \equiv 1$ and the isotopic profile is written in the form of Equation (16), but with the diffusion length given by $\sigma_J = \sqrt{2f_J D_s t}$, wherein the enhancement factor is $f_J = 1 + \phi D_v/D_s$ and $\phi = a^2/b^2$ is the porosity. By including the effect of diffusion through the solid phase along the axial concentration gradient, described by the second term on the right of Equation (18), we have ensured that the diffusion length σ_J does depend weakly on the solid-state diffusivity and the enhancement factor approaches unity at zero liquid fraction. The Johnsen model accounts for misorientations between the vein axis and the direction of the prevailing isotopic gradient by replacing the vein diffusivity with D_v/τ_1, where τ_1 is the tortuosity factor. For the modeled geometry, $\tau_1 = 1$; later, we show the behavior predicted by our model for an isotropic distribution of vein orientations so that D_v is reduced by $\tau_1 = 3$.

2.1.3. Model comparison

We adopt parameter values that are representative of the conditions sampled by ice cores. The outer radius b is chosen to correspond to a typical grain-size so that $b = 10^{-3}$ m. The inner radius a is chosen to be typical of expected vein sizes so that $a = 10^{-6}$ m. The average of the measured diffusion parameters reported by Ramseier (1967) is used to calculate the temperature-dependent molecular diffusivity from

$$D_s = 9.1 \times 10^{-4} \exp\left(-\frac{7.2 \times 10^3}{T}\right) \text{ m}^2 \text{s}^{-1}, \quad (19)$$

where T is the absolute temperature. For the liquid diffusivity, the experimental data reported by Gillen and others (1972) for supercooled water at temperatures down to 242 K are fit to a quadratic given by

$$D_v = \left(1.728 \times 10^{-8} - 1.575 \times 10^{-10} T + 3.591 \times 10^{-13} T^2\right) \text{ m}^2 \text{s}^{-1}. \quad (20)$$

The temperature in the upper part of the GRIP core is approximately 241 K; using this as a nominal value, the diffusivities are $D_s \approx 9.6 \times 10^{-17}$ m^2 s^{-1} and $D_v \approx 1.8 \times 10^{-10}$ m^2 s^{-1}.

The annual-layer thickness decreases with depth, and accumulation rates vary widely, so the axial length scale for isotopic variations is highly sample-dependent. Figure 2 shows the predictions of the three models for the enhancement factor f as a function of wavelength. This is the factor by which the apparent diffusivity of the solid–liquid mixture exceeds that of single ice crystals. For isotopic signals with short wavelengths, our model predictions (solid line) follow those of the Nye model (dot-dashed line), which increases from unity by an amount proportional to the square of the wavelength. At longer wavelengths, the enhancement tends to the horizontal asymptote predicted by the Johnsen model (dashed line). The dotted line shows the predicted enhancement when the liquid diffusivity is reduced by a tortuosity factor of $\tau_1 = 3$.

A closer examination of the transcendental Equation (14) for k_r reveals that the dimensionless parameter

$$\Upsilon \equiv abk_z^2 \frac{D_v}{D_s} = \phi^{1/2} \frac{D_v}{D_s} \frac{4\pi^2 b^2}{\lambda^2}. \quad (21)$$

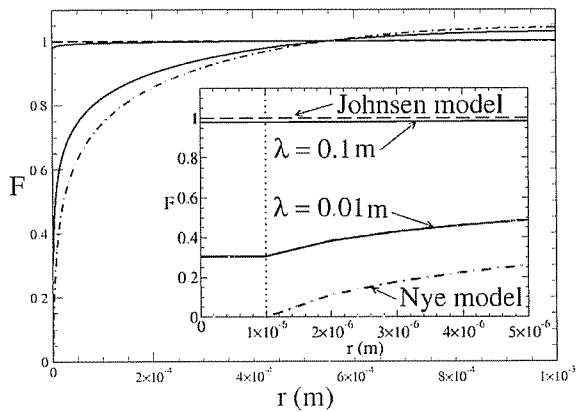is diagnostic of the regime with which the model predictions

Fig. 3. *Normalized isotopic profiles* $F = (\delta - \delta_0)/(\bar{\delta} - \delta_0)$ *as a function of radial position. The inset shows a close-up near the vein wall (vertical dotted line). Model profiles (solid lines) are shown for signal wavelengths of* $\lambda = 0.1\,m$ *and* $\lambda = 0.01\,m$, *labeled in the inset. The Nye (dot-dashed line) and Johnsen (dashed line) model radial profiles are independent of* λ. *Calculations were performed using the nominal parameter values of* $T = 241\,K$, $a = 10^{-6}\,m$ *and* $b = 10^{-3}\,m$.

Fig. 4. *The enhancement factor as a function of the grain-size* b *(*$T = 241\,K$ *and* $a = 10^{-6}\,m$*). Predictions for the present model and the Nye model are shown for wavelengths of* $\lambda = 0.1$ *and* $0.01\,m$. *The Johnsen model is insensitive to wavelength.*

are most closely associated. Physically, Υ can be thought of as a measure of the relative efficiency of isotopic transport through the fluid compared to isotopic exchange between the phases. We expect the radial wavenumber k_1 to be largely controlled by the grain-size so that $k_1 = O\left(b^{-1}\right)$ and to leading order in a/b Equation (14) can be approximated as

$$
J_1(k_1 a) Y_1(k_1 b) - J_1(k_1 b) Y_1(k_1 a)
$$
$$
\approx -\frac{\Upsilon}{2bk_1}[J_0(k_1 a) Y_1(k_1 b) - J_1(k_1 b) Y_0(k_1 a)]. \tag{22}
$$

At small wavelengths, Υ is large (i.e. $\Upsilon \approx 7 \times 10^2$ for $\lambda = 0.01\,\text{m}$ using the nominal parameter values described above) and Equation (22) reduces to Equation (17) derived for the Nye model. At large wavelengths, Υ is more modest in size (i.e. $\Upsilon \approx 7$ for $\lambda = 0.1\,\text{m}$) and the behavior predicted by Equation (22) tends closer to the Johnsen-model results.

Further intuition into the physical processes that control the model behavior is gained by examining the radial isotopic profiles, shown in Figure 3. In the Johnsen model (dashed line) equilibrium is assumed so the isotope concentration is equal to the radial average throughout and $F_J \equiv 1$. In the Nye model (dot-dashed line) the diffusivity of the fluid is infinite so the isotope concentration at the vein wall is equal to the vertical average and $F_N(a) = 0$. The region near the vein wall is expanded in the figure inset, which shows that the present model (labeled solid lines) predicts an isotope concentration at the vein wall (vertical dotted line) approaching unity for $\lambda = 0.1\,\text{m}$. When the length scale of axial isotopic variations is relatively large, the concentration gradient that drives diffusion through the fluid is small, and exchange between the solid and liquid easily replenishes the isotopic content of the veins so that it stays near the radially averaged value. At a wavelength of $\lambda = 0.01\,\text{m}$ our model profile is more similar to that predicted by the Nye model. The shorter wavelength produces larger axial concentration gradients that deplete the isotope concentration in the veins more rapidly than diffusion through the solid can resupply it; to compensate, the isotope concentration at the vein wall drops so that the axial gradient is reduced
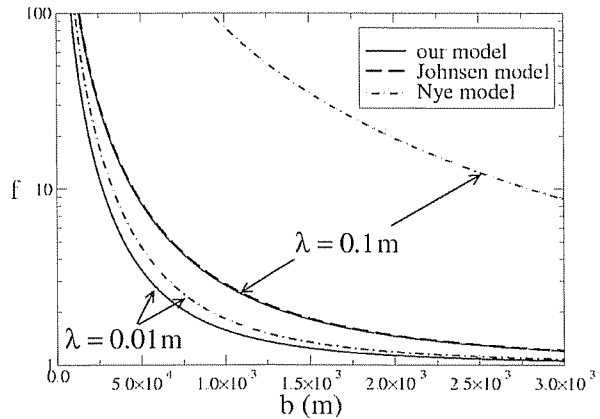
and the radial gradient through the solid is increased. Further analysis shows that the enhancement factor can be written as $f \approx 1 + \phi F(a) D_v/D_s$ when Equation (22) holds; this form highlights the connection between our model predictions and those of the Johnsen model, for which $F(a) = 1$.

Figure 4 shows that all three models are sensitive to the grain-size b. For the Johnsen model, a decrease in b implies an increase in the volume fraction of liquid $\phi = a^2/b^2$ and the efficiency of axial transport is increased. In the Nye model, a drop in b reduces the distance for transport through the solid so that the enhancement rises. The present model embodies both of these effects; demonstrating the dominance of radial transport for short-wavelength signals (large Υ) and changes in liquid volume fraction for long-wavelength signals (smaller Υ). In addition to affecting the porosity and the distance for radial transport, changes in grain-size alter the value of the dimensionless parameter Υ. Holding all else constant, Υ increases with b so we expect smaller grain-sizes to tend increasingly toward the Johnsen-model predictions and larger grain-sizes to promote behavior that approaches closer to the Nye-model results. Since the Nye model and the Johnsen model each neglect part of the transport process, they both represent upper bounds on the rate of isotopic diffusion predicted by our model.

At the temperatures present in polar cores, the volume fraction of pre-melted liquid is expected to be dominated by the effect of impurities in lowering the equilibrium melting temperature (Rempel and others, 2002). For typical impurity loadings and grain-sizes of order $10^{-3}\,\text{m}$, this implies that vein radii are of order $10^{-6}\,\text{m}$. Impurity concentrations change over length scales that are comparable to λ and are correlated with changes in grain-size (Thorsteinsson and others, 1997); to satisfy equilibrium requirements (Mader, 1992a; Nye, 1992) the vein radii are expected to remain relatively uniform over much larger distances. In Figure 5, the enhancement predicted by the Johnsen model is shown to increase at a rate proportional to a^2 since this is the degree by which the liquid fraction ϕ increases with vein radius. The Nye model is only modestly affected by changes to a, since an increase to the vein radius has a proportionately modest effect on the radial distance for isotopic transport and exchange between the phases. The enhancement predicted by the current model is tracked in the behavior of the Johnsen model at small vein radii, which correspond to smaller values of Υ. Our predicted
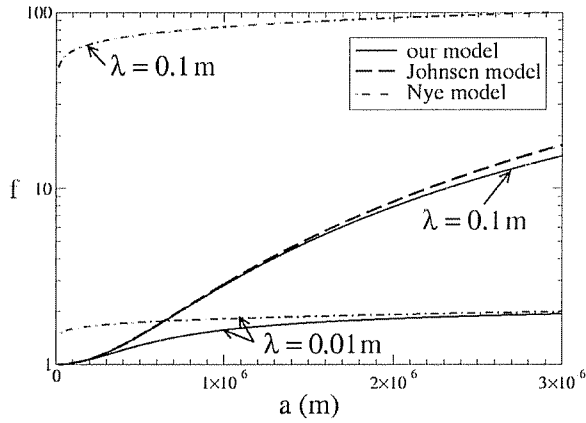
Fig. 5. The enhancement factor as a function of the vein size a ($T = 241\,K, b = 10^{-3}\,m$, λ as labeled).
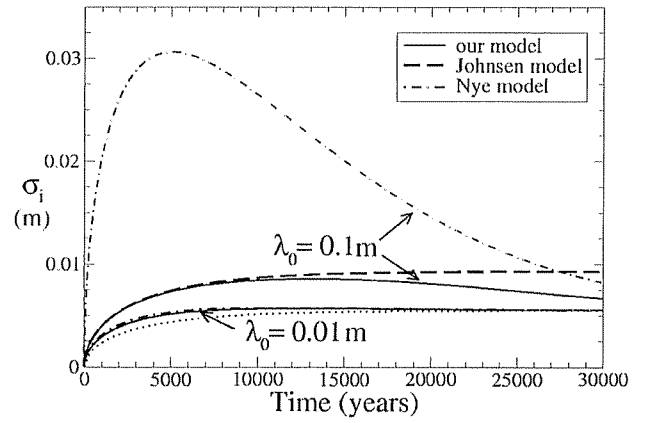

Fig. 6. The evolution of the diffusion length for the generalized model (solid lines), the Nye model (dot-dashed lines) and the Johnsen model (dashed lines) at the labeled initial wavelengths. The dotted line shows the diffusion length predicted for a homogeneous medium with diffusivity D_s. All calculations performed using the nominal parameter values of $T = 241\,K$, $b = 10^{-3}\,m$ and $a = 10^{-6}\,m$ at a constant strain rate of $\dot{\epsilon} = -10^{-4}\,year^{-1}$.

enhancement approaches the Nye-model result asymptotically at larger vein radii, as shown by the solid curve for $\lambda = 0.01$ m.

2.2. A generalized model

The isotope records sampled by ice cores are not simple harmonic signals, but instead are characterized by variations that span a range of wavelengths. The initial isotopic profile at the base of the firn, immediately after pore close-off, can be expressed as a sum of M harmonic components

$$\bar{\delta}_{t=0} = \delta_0 + \sum_{i=1}^{M}[\delta_{ic}\cos(k_{zi0}z) + \delta_{is}\sin(k_{zi0}z)], \quad (23)$$

with initial wavenumbers $k_{zi0} = 2\pi/\lambda_{i0}$, wavelengths λ_{i0}, and amplitudes δ_{ic} and δ_{is}. In addition to diffusive smoothing, the effects of vertical strain must be accounted for if inversion techniques are to be used to recover the original isotopic profiles. For a uniform vertical strain rate $\dot{\epsilon} < 0$, the equation that describes the evolution of the isotopic profiles is

$$\frac{\partial\delta}{\partial t} = D_s\left(\frac{\partial^2\delta}{\partial r^2} + \frac{1}{r}\frac{\partial\delta}{\partial r} + \frac{\partial^2\delta}{\partial z^2}\right) - \dot{\epsilon}z\frac{\partial\delta}{\partial z}. \quad (24)$$

In the ice sheets, recrystallization processes act to ensure that the effects of strain do not significantly alter the geometry of grains as a function of depth (Thorsteinsson and others, 1997). We assume that the diffusive exchange of isotopes between the solid and the liquid is sufficiently rapid that horizontal strain has a negligible effect on the radial isotopic profiles. In this limit, the boundary conditions given by Equations (10) and (11) apply to the solution of the generalized model as well. The solution to Equation (24), subject to Equations (10), (11) and (23), is

$$\delta = \delta_0 + \sum_{i=1}^{M} F_i(r)\left[\delta_{ic}\cos(k_{zi}z)\right.$$
$$\left. + \delta_{is}\sin(k_{zi}z)\right]\exp\left(-\frac{1}{2}k_{zi}^2\sigma_i^2\right), \quad (25)$$

where the ith axial wavenumber is $k_{zi} = 2\pi/\lambda_i$ and the evolution of its wavelength is described by $\lambda_i = \lambda_{i0}\exp\left(\int_0^t \dot{\epsilon}\,d\tau\right)$. Each harmonic component is attenuated to a degree that

depends on the diffusion length σ_i for that portion of the signal, where

$$\sigma_i^2 = 2\exp\left(\int_0^t 2\dot{\epsilon}\,d\tau\right)\int_0^t \left[f_i D_s \exp\left(-\int_0^\tau 2\dot{\epsilon}\,d\eta\right)\right]d\tau, \quad (26)$$

with the ith enhancement factor defined as $f_i = 1 + k_{ri}^2/k_{zi}^2$ and each k_{ri} satisfying Equation (14). The normalized radial profile for each component $F_i(r)$ is described by Equation (15).

For physical insight, it is useful to compare the model behavior to that predicted in the limiting cases where the enhancement factor is adequately described by either the Nye model or the Johnsen model. Taking the case of a constant vertical strain rate, the Johnsen-model enhancement factor is substituted into Equation (26) to predict a diffusion length from

$$\sigma_J^2 = -\frac{D_s}{\dot{\epsilon}}\left(1 + \frac{a^2 D_v}{b^2 D_s}\right)[1 - \exp(2\dot{\epsilon}t)], \quad (27)$$

which is independent of wavelength. At long times, the exponential term tends to zero ($\dot{\epsilon} < 0$) and the diffusion length approaches a steady state, with the tendency for diffusion to increase σ exactly balanced by the effects of vertical strain. In the Nye-model regime, the enhancement factor is inversely proportional to k_{zi}^2 and the diffusion length for a constant vertical strain rate is given by

$$\sigma_{iN}^2 = -\frac{D_s}{\dot{\epsilon}}[1 - \exp(2\dot{\epsilon}t)] + 2D_s\frac{k_N^2}{k_{zi0}^2}t\exp(2\dot{\epsilon}t), \quad (28)$$

where the final term is written in terms of the initial wavenumber so that the time dependence is made explicit. At long times, the exponential terms decay and the diffusion length approaches the value that would be predicted for a homogeneous medium with diffusivity D_s.

Figure 6 shows the evolution of the diffusion length calculated from Equation (26) with a vertical strain rate of $\dot{\epsilon} = -10^{-4}\,a^{-1}$ (chosen to correspond to $\dot{\epsilon} \approx -\dot{h}/H$, where the accumulation rate is $\dot{h} = 0.3\,m\,a^{-1}$ and the ice-sheet thickness is $H = 3000\,m$). For a harmonic signal with an initial wavelength of 0.01 m, the generalized model agrees with the predictions of the Nye model, with the diffusion length
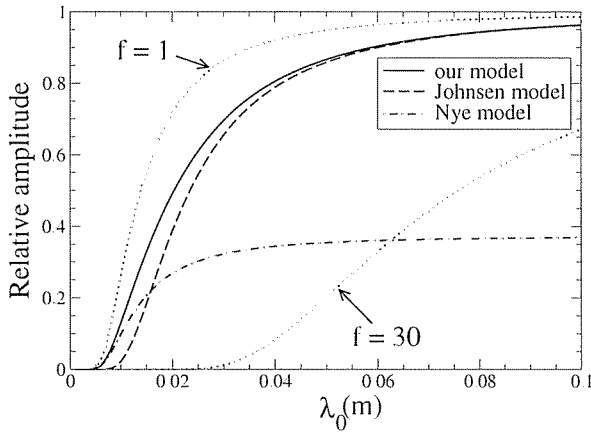
Fig. 7. The predicted amplitudes of harmonic signals after 1000 years, measured relative to their initial amplitudes and plotted as a function of their initial wavelengths. The dotted lines show the amplitudes that would be predicted for constant enhancements of $f = 1$ and $f = 30$. All calculations performed using $T = 241\,K$, $b = 10^{-3}\,m$, $a = 10^{-6}\,m$ and $\dot{\epsilon} = -10^{-4}\,year^{-1}$.
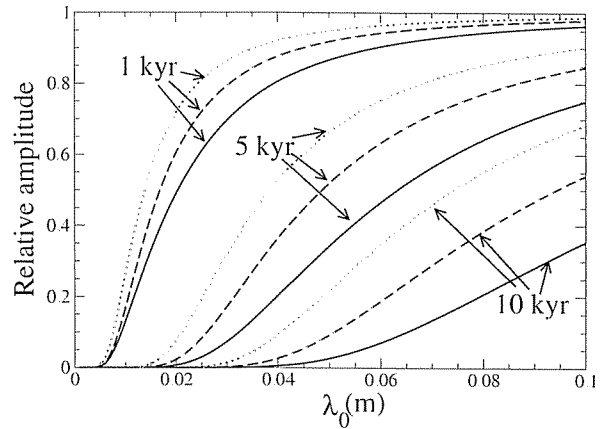

Fig. 8. The predicted amplitudes of harmonic signals after the labeled time intervals, measured relative to their initial amplitudes and plotted as a function of their initial wavelengths. The solid lines show the amplitudes predicted using the nominal parameter values. The dashed lines show the predicted amplitudes when the liquid diffusivity is reduced by a tortuosity factor of $\tau_f = 3$. The dotted lines show the amplitudes that would be predicted for a homogeneous medium with the solid-state monocrystalline diffusivity.

increasing rapidly to a maximum of just over 0.5 cm, before dropping slightly at later times. For an initial wavelength of 0.1 m, the predicted diffusion length tracks the Johnsen-model results at first, then decreases as strain reduces the wavelength and puts the system into the Nye-model regime. The tendency for the diffusion length to reach a maximum at intermediate times rather than increase monotonically to a constant asymptote is a significant qualitative difference between our model predictions and the behavior expected for a homogeneous single-phase medium. Vertical strain eventually reduces the wavelength sufficiently that the Nye-model regime is reached, and at later times the diffusion length tends to the asymptote that would be predicted for a homogeneous medium with the diffusivity of solid ice (dotted line). This behavior is consistent with the observation of a large excess diffusion in the Holocene ice at GRIP, whereas the annual signals in the Wisconsin ice are attenuated much more slowly.

The attenuation of harmonic signals is shown as a function of their initial wavelengths in Figure 7. Results are presented in terms of their amplitudes after a time interval of 10^3 years, relative to their initial amplitudes. The predictions of the Nye model follow ours for short wavelengths. The Nye-model predictions tend to a horizontal asymptote of approximately 0.38 at larger wavelengths; the Johnsen-model results are more closely identified with those of our model in the large-wavelength regime. The relative amplitudes predicted by our model are always somewhat higher than those predicted by both the Johnsen and Nye models. The dotted line labeled $f = 1$ shows the attenuation that would be achieved in a homogeneous medium with the solid-state monocrystalline diffusivity D_s. The observations from GRIP Holocene ice reported by Johnsen and others (1997) are consistent with a diffusivity that is approximately 30 times greater than D_s; the dotted line labeled $f = 30$ shows the signal strength that is calculated using this enhancement factor. Figure 8 compares the predicted signal attenuation with the attenuation that would be expected for a homogeneous medium with the solid-state monocrystalline diffusivity D_s, after the labeled time periods. Also

shown are predictions in which the veins are assumed to be randomly oriented with respect to the prevailing isotopic gradient, so that the effective liquid diffusivity is D_v/τ_f, where the tortuosity factor is $\tau_f = 3$.

3. THE CAUSES OF EXCESS DIFFUSION

The model we have presented clearly demonstrates the importance of pre-melted liquid in enhancing the rate of isotopic diffusion in polar ice. Its effect on the relative amplitudes of isotopic signals is illustrated in Figure 8 by the differences between the dotted lines and the solid and dashed lines that represent our model predictions for $\tau_f = 1$ and $\tau_f = 3$. However, Figure 7 shows that the predicted amplitudes for conditions similar to those encountered in the Holocene ice at GRIP are considerably higher than those observed by Johnsen and others (1997), which are represented by the dotted line calculated using their inferred enhancement of $f = 30$ (Johnsen and others, 2000). The predicted enhancement can be increased by decreasing the model grain-size (see Fig. 4) or increasing the model vein size (see Fig. 5), but it is difficult to explain such rapid attenuation without invoking a much higher liquid fraction than is commonly believed. We have considered only the contribution from the bulk colligative effects of soluble impurities and have not considered that intermolecular forces can cause liquid films to form on grain boundaries. Although such grain-boundary melting takes place on a smaller length scale than accessed using typical optical methods, the large surface area involved can result in a significant volume of interfacial pre-melted liquid. In addition to promoting enhanced rates of diffusive transport through the veins, a higher liquid fraction would tend to increase the importance of advective fluid transport, as discussed in the Appendix. Other sources of the apparent discrepancy between the model predictions and ice-core observations require further consideration, discussed presently.

3.1. Liquid geometry

The model is formulated for an idealized geometry that does not capture all the subtle features that characterize the pre-melted-liquid network in polycrystalline ice. To test the sensitivity of the model predictions to the grain-scale geometry, we examined an inverted model in which a cylinder of solid ice with radius b is enclosed by a thin film of liquid with thickness d. The inner radius b is identified with the grain-size, and the film thickness d is chosen so that the liquid fraction $\phi \approx 2d/b$ matches that of our original model. For signals with longer wavelengths, the predictions of the inverted model and the original model are identical. This reflects the asymptotic behavior of our model at small Υ, which yields predictions that are in agreement with those of the Johnsen model and depend on the liquid volume-fraction. At shorter wavelengths, in the Nye-model regime, the inverted model and the original model differ slightly in detail, but show the same qualitative behavior. As noted earlier, our predicted enhancement is bounded above by that of both the Johnsen and Nye models. Since the idealized model geometry does not cause a reduction in the Johnsen-model enhancement, which is itself much lower than the enhancement inferred from the GRIP Holocene ice, we conclude that there must be another reason why the model predicts a weaker enhancement than is observed.

3.2. Grain-size variations

The model is formulated for polycrystalline ice with a constant grain-size and vein size. Theoretical considerations (Nye, 1992) and laboratory observations (Mader, 1992b) indicate that the vein size should be fairly uniform. The same is not true for grain-sizes, which are anticorrelated with the impurity loading and vary over length scales that are commensurate with those of the annual layering (Thorsteinsson and others, 1997). The effects of this variation can be explored with a continuum model that includes variations in liquid volume fraction ϕ. Consider the evolution of the average isotope concentration $\bar{\delta}$ in a control volume that is large in comparison to the grain-size b, but small in comparison to λ. The isotope concentration in the liquid is $F_v \bar{\delta}$, where the scaling factor $1 > F_v > 0$ is determined by the geometry of the liquid network; in the idealized geometry considered above, $F_v = F(a)$. To leading order in ϕ, the evolution of the isotopic profiles is given by

$$\frac{\partial \bar{\delta}}{\partial t} = D_s f \frac{\partial^2 \bar{\delta}}{\partial z^2} - \dot{\epsilon} z \frac{\partial \bar{\delta}}{\partial z} + D_s \frac{\partial f}{\partial z} \frac{\partial \bar{\delta}}{\partial z}, \qquad (29)$$

where the enhancement factor is $f = 1 + \phi F_v D_v / (\tau_l D_s)$, and the tortuosity factor τ_l is included explicitly. Variations in grain-size cause variations in the liquid volume fraction ϕ and scaling factor F_v, and lead to gradients in the enhancement factor that produce the third term on the right side of Equation (29). This additional term alters the character of the solution to Equation (29) so that it cannot be written in the same form as we have used for our earlier model. Gradients in f cause different portions of a harmonic signal to diffuse at different rates so that the signal shape is altered in a complicated manner. Depending on their spatial dependence, variations in grain-size could either enhance or reduce the amplitudes inferred for the annual isotopic signals. Further efforts to quantify this effect will require a careful comparison of the spatial relationships between grain-size variations and changes in isotope concentration. At the pres-

ent stage, a parametric study within the general framework described here would extend beyond the level constrained by firm observational evidence of these controlling effects. Nevertheless, in its current form, the model provides useful guidance for data analysis and interpretation.

3.3. Physical properties

One further possibility that must be considered is whether errors in the physical properties that are used by the model, in particular the diffusivities of the solid and the liquid, might be partly responsible for the apparent diffusion excess. The diffusivity D_v was measured in a pure, supercooled liquid (Gillen and others, 1972), whereas the pre-melted liquid is in equilibrium, mainly due to the presence of impurities. Impurity ions in solution are surrounded by hydration shells in which the mobility of the water molecules is reduced. Hence, the presence of impurities should tend to make the effective liquid diffusivity lower than that found in supercooled liquid. This suggests that the predicted enhancement can be reduced by the presence of impurities, but it is unlikely to be increased.

The diffusivity of the solid D_s was measured on single ice crystals (Ramseier, 1967). Solid-state diffusion in ice involves the motion of point defects, primarily vacancies, so one might expect processes that alter the concentration of point defects to also produce changes to D_s. We are not aware of any systematic measurements of D_s in ice that has been strained, confined at elevated pressures, or doped with the impurity molecules, NH_3, F^- and Cl^-, that are known to form substitutional defects in the ice lattice. Evidence to support the view that the diffusivity measured by Ramseier (1967) might be lower than that which applies to the polar ice-core record comes from a consideration of isotopic diffusion in the firn. Models for firn diffusion (Johnsen, 1977; Whillans and Grootes, 1985) have been remarkably successful (Cuffey and Steig, 1998) despite their assumption of isotopic equilibrium between the solid and vapor phases. As Johnsen and others (2000) note, and a simple adaptation of our model shows, the exchange of isotopes by diffusion between the solid and vapor would be too slow to make this assumption valid if the Ramseier (1967) diffusivity D_s applies. While it is possible that recrystallization processes enhance the isotopic exchange in the firn and explain the rapid equilibration (Johnsen and others, 2000), a higher diffusion coefficient for the solid is an alternative explanation. We note that, for all but the signals with the shortest wavelengths, our model predicts that the solid and liquid beneath the firn are nearly in isotopic equilibrium so recrystallization processes cannot increase the enhancement above that which we predict.

4. CONCLUSIONS

The stable-isotope records that are recovered from ice cores represent invaluable archives of past temperatures. The accuracy of the paleothermometry that derives from such records relies on a proper treatment of processes that affect the isotope profiles during their long residence times in an ice sheet. The model that has been presented here quantifies the role that diffusion through pre-melted liquid plays in enhancing the rate of isotopic smoothing beneath the firn. The process can be subdivided into two steps: (1) exchange of isotopes between the solid grains and the pre-melted liquid, and (2) rapid diffusion through the liquid along the dominant isotope-concentration gradient. Both processes

must be accounted for in a complete description of the diffusive smoothing of isotopic signals, and each comes to the fore as the dominant control on the rate of diffusive smoothing in a different parameter regime. When grains are larger and wavelengths are shorter, the lateral exchange of isotopes is the slower, rate-limiting process. In this parameter regime, the isotopic content of the solid grains is laterally inhomogeneous, emphasizing the requirement that sample volumes contain many grains in order to provide representative measurements. When the grains are smaller and wavelengths are longer, pre-melted liquid is most effective at enhancing the rate of diffusion so that isotopic exchange is rapid and the speed of axial transport controls the diffusive smoothing. In this parameter regime, the efficiency of axial transport increases in proportion to the volume fraction of liquid that is present. This implies that variations in impurity loading, which are anticorrelated with variations in grain-size, should produce variations in the rate of axial transport and alter the harmonic content of isotopic signals. This behavior may be responsible for the apparent diffusivity inferred from the GRIP Holocene ice being larger than our model predicts. Alternative explanations that we have explored include the possibility that the liquid fraction is larger than is commonly believed, or that, due to defect-scale phenomena, the solid-state diffusivity in the ice sheets is larger than the laboratory-measured value.

ACKNOWLEDGEMENTS

REFERENCES

Bolzan, J. F. and V. A. Pohjola. 2000. Reconstruction of the undiffused seasonal oxygen isotope signal in central Greenland ice cores. *J. Geophys. Res.*, **105**(C9), 22,095–22,106.

Cho, C. H., J. Urquidi, S. Singh and G. W. Robinson. 1999. Thermal offset viscosities of liquid H_2O, D_2O, and T_2O. *J. Phys. Chem.*, **103**(11), 1991–1994.

Cuffey, K. M. and E. J. Steig. 1998. Isotopic diffusion in polar firn: implications for interpretation of seasonal climate parameters in ice-core records, with emphasis on central Greenland. *J. Glaciol.*, **44**(147), 273–284.

Dansgaard, W. 1964. Stable isotopes in precipitation. *Tellus*, **16**(4), 436–468.

Dash, J. G., H.-Y. Fu and J. S. Wettlaufer. 1995. The premelting of ice and its environmental consequences. *Rep. Prog. Phys.*, **58**(1), 115–166.

Fisher, D. A. 1987. Enhanced flow of Wisconsin ice related to solid conductivity through strain history and recrystallization. *International Association of Hydrological Sciences Publication* 170 (Symposium at Vancouver 1987 — *The Physical Basis of Ice Sheet Modelling*), 45–51.

Gillen, K. T., D. C. Douglass and M. J. R. Hoch. 1972. Self-diffusion in liquid water to −31 °C. *J. Chem. Phys.*, **57**(12), 5117–5119.

Glen, J. W., D. R. Homer and J. G. Paren. 1977. Water at grain boundaries: its role in the purification of temperate glacier ice. *International Association of Hydrological Sciences Publication* 118 (Symposium at Grenoble 1975 — *Isotopes and Impurities in Snow and Ice*), 263–271.

Johnsen, S. J. 1977. Stable isotope homogenization of polar firn and ice. *International Association of Hydrological Sciences Publication* 118 (Symposium at Grenoble 1975 — *Isotopes and Impurities in Snow and Ice*), 210–219.

Johnsen, S. J. *and 14 others.* 1997. The $\delta^{18}O$ record along the Greenland Ice Core Project deep ice core and the problem of possible Eemian climatic instability. *J. Geophys. Res.*, **102**(C12), 26,397–26,410.

Johnsen, S. J., H. B. Clausen, J. Jouzel, J. Schwander, A. E. Sveinbjörnsdóttir and J. White. 1999. Stable isotope records from Greenland deep ice cores. *In* Wettlaufer, J. S., J. G. Dash and N. Untersteiner, *eds. Ice physics and the natural environment.* Berlin, etc., Springer-Verlag, 89–107. (NATO ASI Series I: Global Environmental Change 56.)

Johnsen, S. J., H. B. Clausen, K. M. Cuffey, G. Hoffmann, J. Schwander and T. Creyts. 2000. Diffusion of stable isotopes in polar firn and ice: the isotope effect in firn diffusion. *In* Hondoh, T., *ed. Physics of ice core records.* Sapporo, Hokkaido University Press, 121–140.

Mader, H. M. 1992a. Observations of the water-vein system in polycrystalline ice. *J. Glaciol.*, **38**(130), 333–347.

Mader, H. M. 1992b. The thermal behavior of the water-vein system in polycrystalline ice. *J. Glaciol.*, **38**(130), 359–374.

Nye, J. F. 1992. Water veins and lenses in polycrystalline ice. *In* Maeno, N. and T. Hondoh, *eds. Proceedings of the International Symposium on the Physics and Chemistry of Ice, Sapporo, Japan.* Sapporo, Hokkaido University Press, 200–205.

Nye, J. F. 1998. Diffusion of isotopes in the annual layers of ice sheets. *J. Glaciol.*, **44**(148), 467–468.

Nye, J. F. and F. C. Frank. 1973. Hydrology of the intergranular veins in a temperate glacier. *International Association of Scientific Hydrology Publication* 95 (Symposium at Cambridge 1969 — *Hydrology of Glaciers*), 157–161.

Ohtomo, M. and G. Wakahama. 1983. Growth rate of recrystallization in ice. *J. Phys. Chem.*, **87**(21), 4139–4142.

Petit, J.-R. *and 18 others.* 1999. Climate and atmospheric history of the past 420,000 years from the Vostok ice core, Antarctica. *Nature*, **399**(6735), 429–436.

Phillips, O. M. 1991. *Flow and reactions in permeable rocks.* Cambridge, Cambridge University Press.

Ramseier, R. O. 1967. Self-diffusion of tritium in natural and synthetic ice monocrystals. *J. Appl. Phys.*, **38**(6), 2553–2556.

Raymond, C. F. and W. D. Harrison. 1975. Some observations on the behavior of the liquid and gas phases in temperate glacier ice. *J. Glaciol.*, **14**(71), 213–233.

Rempel, A. W. and J. S. Wettlaufer. 2003. Segregation, transport and interaction of climate proxies in polycrystalline ice. *Can. J. Phys.*, **81**(1–2), 89–97.

Rempel, A. W., E. D. Waddington, J. S. Wettlaufer and M. G. Worster. 2001. Possible displacement of the climate signal in ancient ice by premelting and anomalous diffusion. *Nature*, **411**(6837), 568–571.

Rempel, A. W., J. S. Wettlaufer and E. D. Waddington. 2002. Anomalous diffusion of multiple impurity species: predicted implications for the ice core climate records. *J. Geophys. Res.*, **107**(B12), 2330. (10.1029/2002JB001857.)

Thorsteinsson, Th., J. Kipfstuhl and H. Miller. 1997. Textures and fabrics in the GRIP ice core. *J. Geophys. Res.*, **102**(C12), 26,583–26,599.

Wettlaufer, J. S. 1999. Impurity effects in the premelting of ice. *Phys. Rev. Lett.*, **82**(12), 2516–2519.

Wettlaufer, J. S. and J. G. Dash. 2000. Melting below zero. *Sci. Am.*, **282**(2), 34–37.

Whillans, I. M. and P. M. Grootes. 1985. Isotopic diffusion in cold snow and firn. *J. Geophys. Res.*, **90**(D2), 3910–3918.

APPENDIX

COMPARING ADVECTIVE AND DIFFUSIVE TRANSPORT IN VEINS

This appendix resulted from a series of exchanges with J. F. Nye during the review process. The principal aspect of these exchanges that we develop here deals with quantifying the relative importance of advection and diffusion in the redistribution of stable isotopes through the vein system in ice sheets.

A comparison of terms in the advection–diffusion equation that describes transport through the veins leads us to define the Péclet number

$$\mathrm{Pe} = \frac{v \lambda \tau_1}{2\pi D_v} , \qquad (A1)$$

to measure the relative size of these effects. Here, v is the average velocity of the water in the veins, $\lambda/2\pi$ is a characteristic length scale for changes in isotopic concentration, and D_v/τ_1 is the effective molecular diffusivity for a tortuosity factor of $\tau_1 \approx 3$. The advective flux is negligible in com-

parison to the diffusive flux when Pe $\ll$ 1. Here we estimate the range of wavelengths $\lambda < \lambda_c$ that satisfy this condition.

In principle, Darcy's law can be used to obtain the transport velocity $U \equiv v\phi$, but there are no direct measurements of the permeability Π or the liquid pressure gradient in polar glacial ice. Nye and Frank (1973) discuss an idealized vein network in which they express the permeability as $\Pi = \phi^2 (2b)^2 / \chi$ where the proportionality constant is $\chi = 2000$. Although Raymond and Harrison (1975) derive a more general model (see also Phillips, 1991, p. 29–34) that accounts for vein obstructions in temperate ice, the Nye and Frank model provides us with a useful upper bound on Π for a given liquid fraction ϕ. We assume that the pressure gradient driving flow is produced by the difference in density between the vein liquid $\rho_v \approx 10^3 \, \mathrm{kg \, m^{-3}}$ and ice $\rho_s \approx 9.2 \times 10^2 \, \mathrm{kg \, m^{-3}}$ so

that Darcy's law gives $U = \Pi / \nu \, (\rho_v - \rho_s) g$, where $g \approx 10 \, \mathrm{m \, s^{-2}}$ is the acceleration of gravity, and the viscosity at $-30°C$ is $\nu \approx 9 \times 10^{-3} \, \mathrm{Pa \, s}$ (Cho and others, 1999). We set the Péclet number to unity and find that the characteristic wavelength λ_c that divides the two transport regimes is

$$\lambda_c = \frac{\pi \chi \nu D_v}{2\phi b^2 (\rho_v - \rho_s) g \tau_f} . \tag{A2}$$

Realistic parameter values as used throughout this paper are for $b = 10^{-3} \, \mathrm{m}$, $\phi = 10^{-6}$ and a liquid diffusivity of $D_v \approx 1.8 \times 10^{-10} \, \mathrm{m^2 \, s^{-1}}$, yielding $\lambda_c \approx 2 \, \mathrm{m}$. We conclude that the purely diffusive model presented here should be valid for the parameter regime experienced in a wide variety of ice-core settings.